Electronic Supplementary Material (ESI) for Catalysis Science & Technology.

Strontium-induced phase, energy band and microstructure regulating in $Ba_{1-x}Sr_xTiO_3$ photocatalysts for boosting visible-light photocatalytic activity

Yan Han[a)], Shifa Wang[a)]*, Maoyuan Li[a)], Huajing Gao[a)], Mengjun Han[a)], Hua Yang[b)], Leiming Fang [c)]**, Jagadeesha Angadi.V[d)], A.F. Abd El-Rehim[e, f)], Atif Mossad Ali [e, g)], Dengfeng Li[h)]***

[a)] Chongqing Key Laboratory of Geological Environment Monitoring and Disaster Early-warning in Three Gorges Reservoir Area, Chongqing Three Gorges University, Chongqing, Wanzhou, 404000, China.

*e-mail: wangshifa2006@yeah.net (Shifa Wang)

[b)] School of Science, Lanzhou University of Technology, Lanzhou 730050, China.

[c)] Institute of Nuclear Physics and Chemistry, China Academy of Engineering Physics, Sichuan, Mianyang, 621900, China.

**e-mail: flmyaya2008@163.com (Leiming Fang)

[d)] Department of Physics, P.C. Jabin Science College, Hubballi – 580031 Karnataka, India.

[e)] Physics Department, Faculty of Science, King Khalid University, P.O. Box 9004, Abha 61413, Saudi Arabia.

[f)] Physics Department, Faculty of Education, Ain Shams University, P.O. Box 5101, Heliopolis 11771, Roxy, Cairo, Egypt.

[g)] Physics Department, Faculty of Science, Assiut University, Assiut 71516, Egypt.

[h)] School of Science, Chongqing University of Posts and Telecommunications, Nan'an District, 400065 Chongqing, China.

***e-mail: lidf@cqupt.edu.cn (Dengfeng Li)

S1 Eg value of $BaTiO_3$

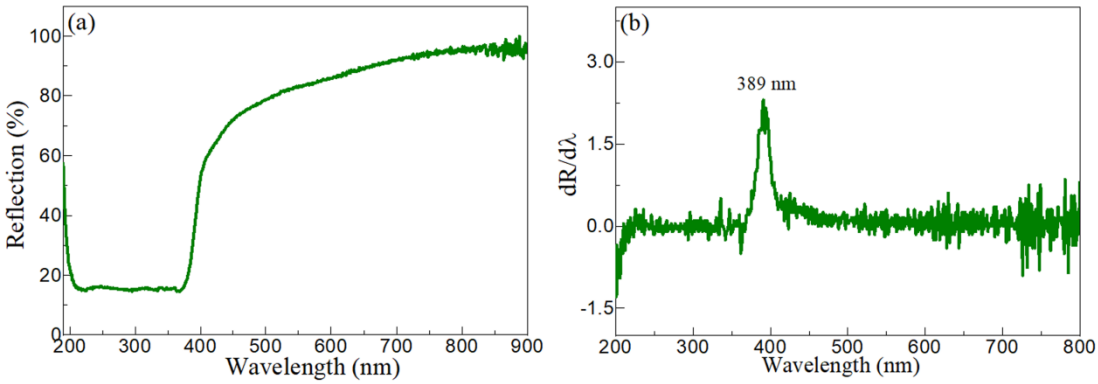

Figure S1 (a) UV-Visible diffuse reflection spectrum and (b) Eg values of $BaTiO_3$ photocatalysts.

Figure S1(a) shows the UV-Visible diffuse reflection spectrum of $BaTiO_3$ photocatalysts. It can be seen from the figure that the reflectance of $BaTiO_3$ photocatalyst decreases sharply in the range of 190-200 nm, remains basically constant in the range of 200-380 nm, and increases with the increase of wavelength in the range of 380-900 nm. The Eg values of $BaTiO_3$ photocatalysts can be calculated by calculating the first differential curve of the UV-Visible diffuse reflection spectrum. The E_g values of $BaTiO_3$ photocatalysts can be estimated by the Equation (S1).

$$E_g(\text{eV}) = \frac{hc}{\lambda_0(\text{nm})} \approx \frac{1240}{\lambda_0(\text{nm})} \quad \text{(S1)}$$

where λ_0 is the position of the peak of the first differential curve. h is the Plank constant and c is the velocity of light. Figure S1(b) shows the Eg values of $BaTiO_3$ photocatalysts. The E_g value of $BaTiO_3$ photocatalysts is 3.19 eV. Compared with $BaTiO_3$, the Eg value of BST photocatalyst has been greatly reduced. Compared with the Eg value of pure $SrTiO_3$ in literature [S1], the Eg value of BST photocatalyst also decreased by at least 0.1 eV.

S2 Effect of catalyst content on photocatalytic activity

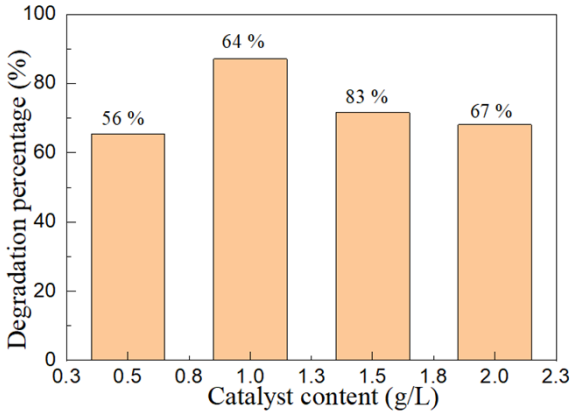

Figure S2 Effect of catalyst content on the photocatalytic degradation of TC-HCl of BST5 photocatalysts under simulated sunlight irradiation.

The degradation rate of TC-HCl as a function of catalyst content as shown in Figure S2. It can be seen that the degradation rate of TC-HCl firstly increases and then decreases with the increasing of the catalyst content. The possible explanation for this phenomenon is that total active surface area increases with the increase of catalyst concentration, so availability of more active sites on BST5 photocatalyst surface. [S2] In addition, as the catalyst content was increased, the penetration of simulated sunlight and photoactivated volume of suspension decreased, hence the degradation percentage of TC-HCl decreases. [S3] However, when the catalyst content excess of 1 g/L, the degradation percentage of TC-HCl reduced due to light scattering [S4]. Therefore, the catalyst content of 1 g/L was fixed for photocatalytic degradation of percentage.

S3 XPS spectra of BST5 photocatalysts after photocatalysis

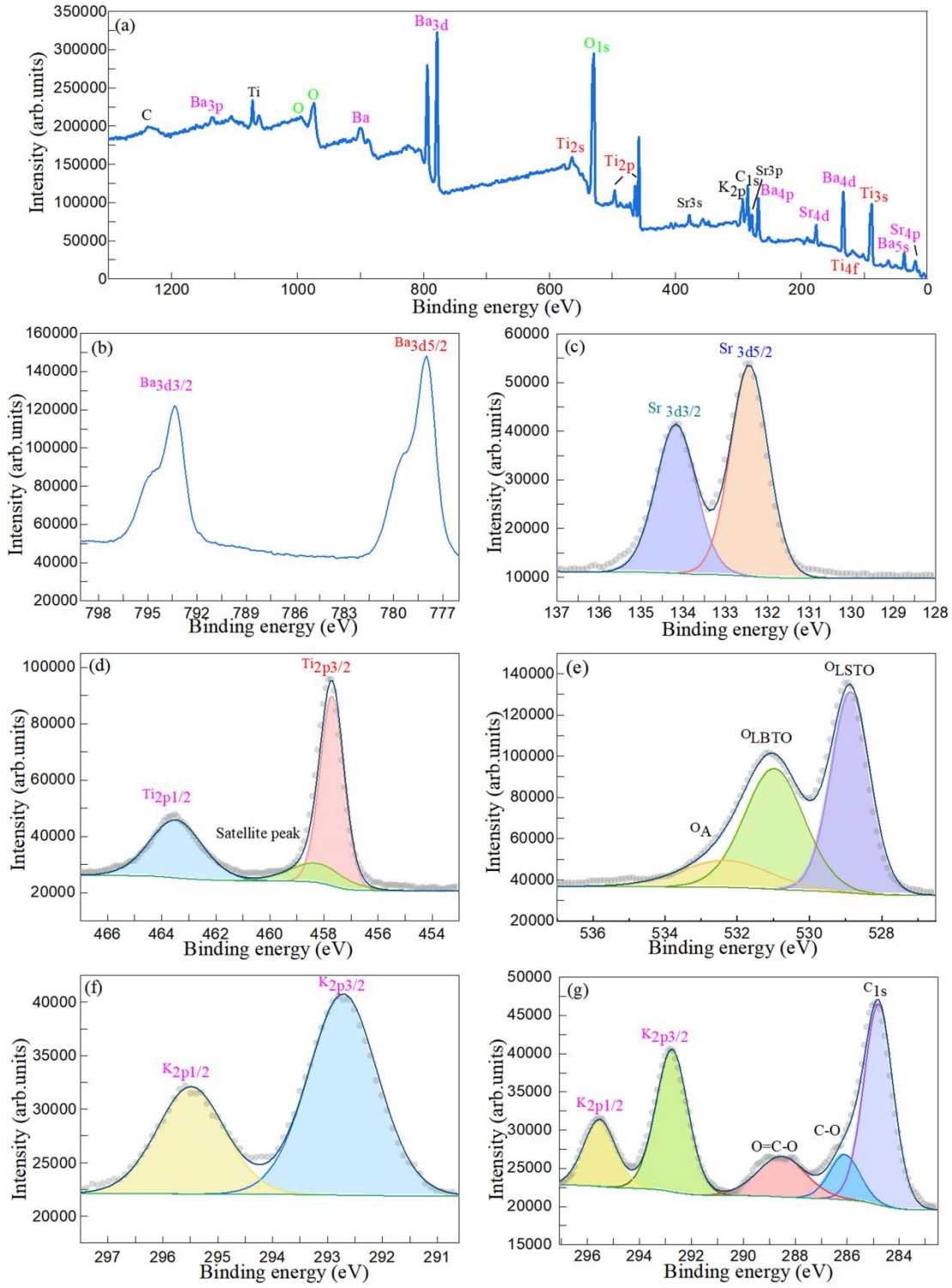

Figure S3 (a) XPS survey scan spectra, (b) Ba 3d, (c) Sr 3d, (d) Ti 2p, (e) O1s, (f) K2p and (g) C1s spectra of BST5 photocatalysts after photocatalysis.

Figure S3 shows the XPS survey scan spectra, Ba 3d, Sr 3d, Ti 2p, O1s, K2p and C1s spectra of BST5 photocatalysts after photocatalysis. As can be seen from the Figure

S3, except for the addition of K2p peak, no peaks of other elements are found, and the positions of peaks of all elements are consistent with those of BST5 photocatalyst before photocatalysis. The K2p peak is mainly caused by the use of KOH before the pH of the reaction solution is adjusted, which further indicates that the BST5 photocatalyst is stable. In addition to the calibration peak, the characteristic peaks of C-O and O=C-O also appear in C1s spectrum. These peaks can be attributed to the small molecular organic matter of carbon remaining on the surface of BST5 photocatalyst after the degradation of TC-HCl.

S4 HPLC-MS analysis

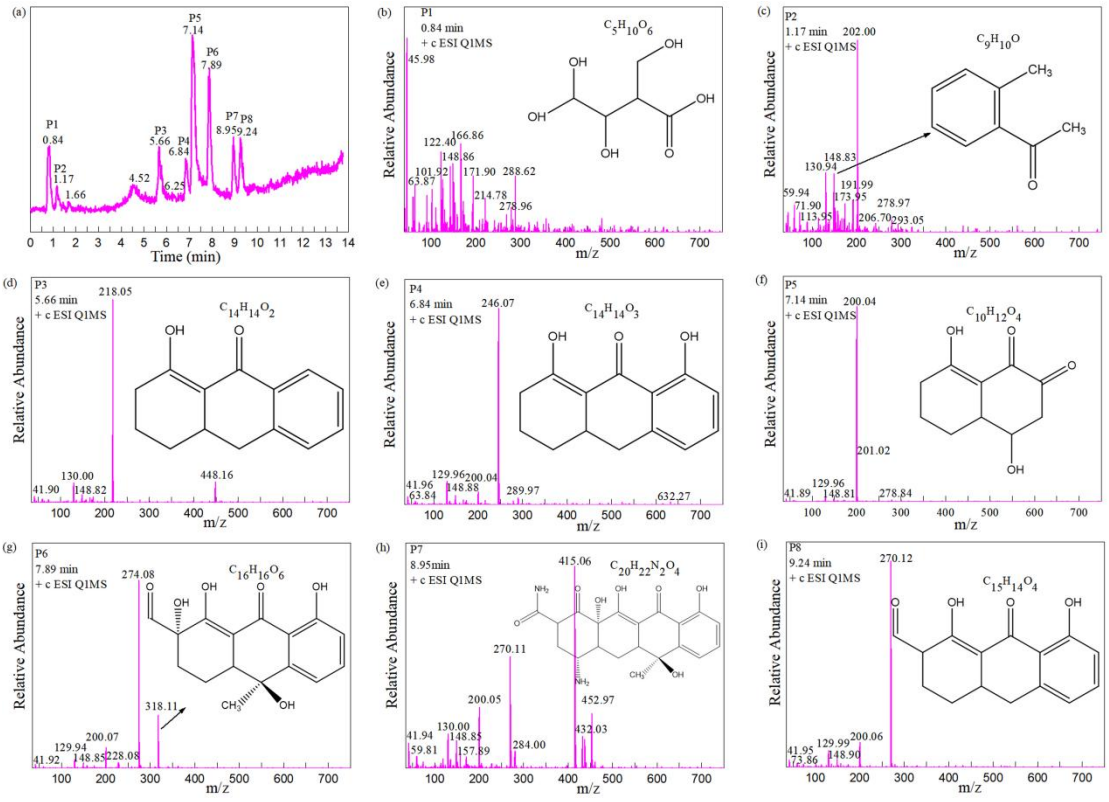

Figure S4 HPLC–MS chromatogram of TC-HCl and the corresponding mass spectra after 15 min of visible-light irradiation by BST5 photocatalysts.

Quantitative analysis of the intermediates for the photocatalytic degradation of TC-HCl by BST5 photocatalysts will be helpful to understand its degradation

mechanism and pathway. HPLC–MS method is an effective method to detect intermediate products of TC-HCl degradation. Figure S4 shows the HPLC–MS chromatogram of TC-HCl and the corresponding mass spectra after 15 min of visible-light irradiation by BST5 photocatalysts. In Figure S4(a), the peaks observed in 0.84, 1.17, 1.66, 4.52, 5.66, 6.84, 7.14, 7.89, 8.95 and 9.24 min were named P1, P2, P3, P4, P5, P6, P7 and P8, respectively. Based on the above analysis, several mass-to-charge ratio (m/z) peaks at 148.86, 166.86, 200.04, 218.05, 246.07, 270.12, 318.11, and 415.06 were observed, indicating the formation of intermediates due to the m/z peak of TC-HCl is 445.43. The relevant molecular and structural formulas are shown in Figure S4(b)-(i). According to these data, the proposed degradation pathway of TC-HCl in the presence of BST5 photocatalysts as shown in Figure S5. In the early stage of degradation, photocatalysis mainly breaks the -CH_3 bond connected with N element and the adjacent -OH in TC-HCl. Subsequently, an open-loop reaction was performed to break the -NH_2 and -$CONH_2$ bonds. The -CH_3 and -OH bonds were further broken when the illumination time continued to increase. The -C=O and -OH were further destroyed to form organic with m/z=246.07. The -OH broke again, forming a polycyclic organics with m/z=218.05. Subsequently, an open-loop reaction is performed that may produce organics with m/z=200.04, m/z=166.86, and m/z=148.86. Eventually, these small molecules break down into CO_2, H_2O and NH_4^+ under continuous illumination.

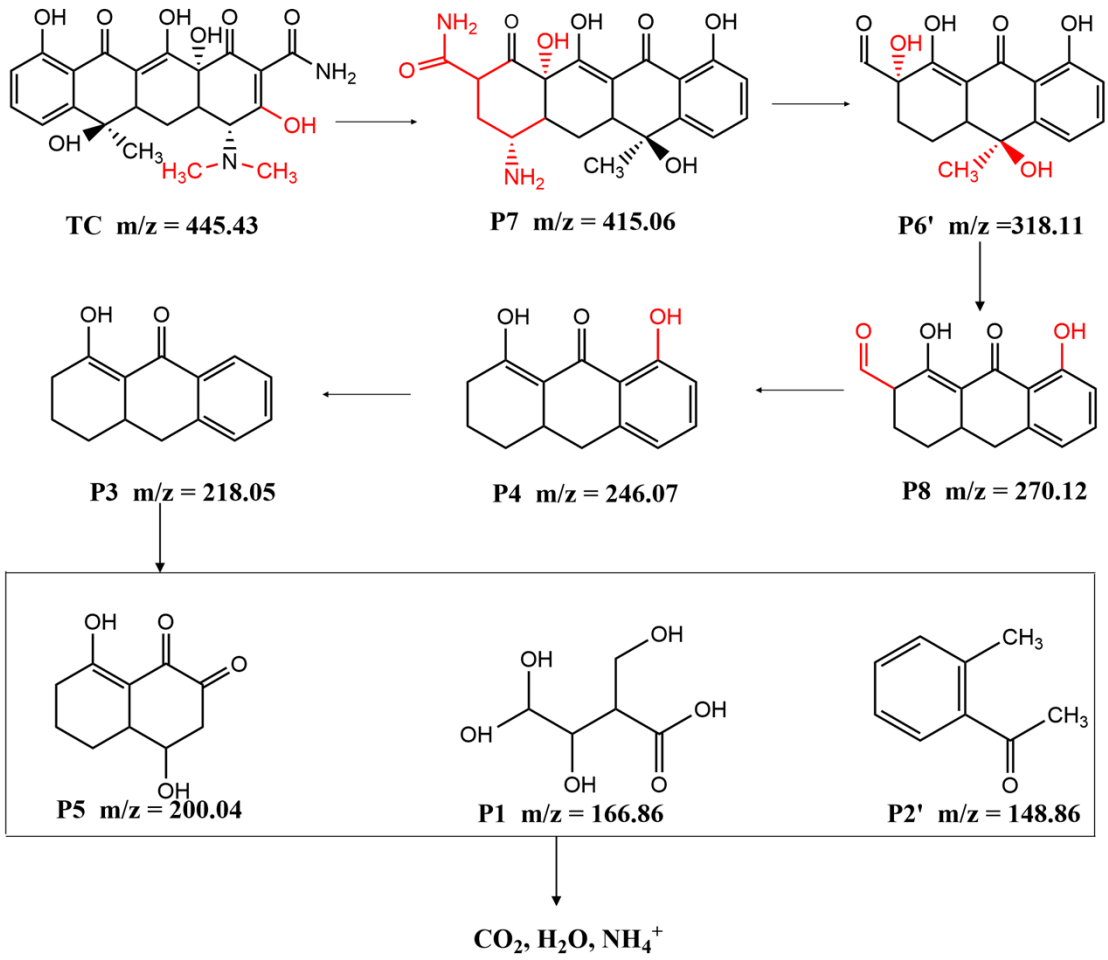

Figure S5 Proposed degradation pathway of TC-HCl in the presence of BST5 photocatalysts.

S4 Toxicity estimation

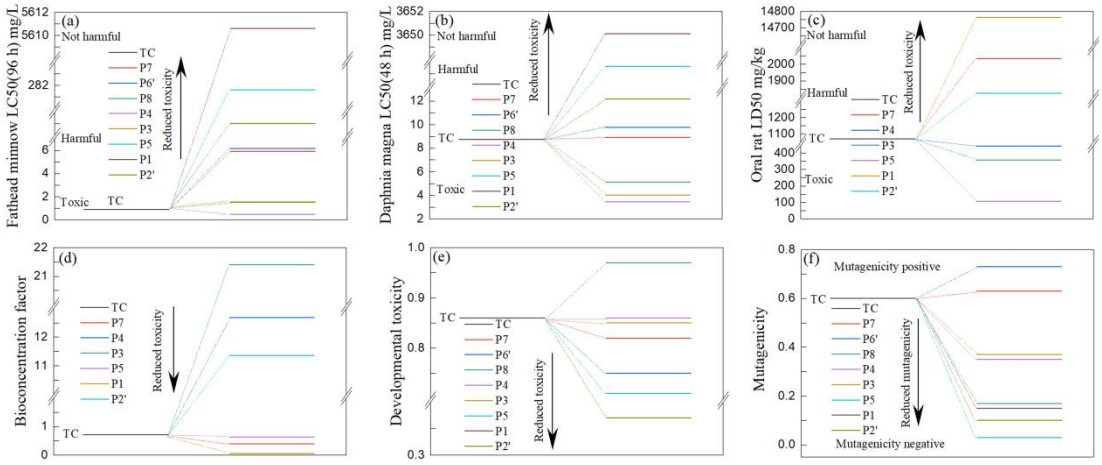

Figure S6 Acute toxicity for the (a) fathead minnow, (b) daphnia magna and (c) oral

rat, (d) bioconcentration factor, (e) development toxicity and (f) mutagenicity of TC-HCl and degradation intermediates.

To exhaustive evaluate the toxicity of TC-HCl and intermediate products, the acute toxicity for the fathead minnow, daphnia magna and oral rat, bioaccumulation factors, developmental toxicity and mutagenicity of TC-HCl and degradation intermediates were detail predicted by the Toxicity Estimation Software Tool (T.E.S.T.) [S5-S7] Figure S6 (a)-(c) shows the acute toxicity for the fathead minnow, daphnia magna and oral rat. Although the toxicity of some intermediates was very high, the toxicity of the final product was reduced, suggesting that the predictions of the three different models were credible. Except for P1, P7 and P5, the bioaccumulative factors of other intermediates are significantly increased as shown in Figure S6(d). With the exception of P8, the developmental toxicity of other intermediates was reduced throughout the removal process as shown in Figure S6(e). In Figure S6(f), TC-HCl, P7 and P6′ are "mutagenic positive", while other intermediates are "mutagenic negitive". By toxicity estimation, the toxicity of some intermediates decreased and some products remained. Therefore, during the photocatalytic degradation of TC-HCl by BST5 photocatalysts, the illumination time should be extended to reduce the toxicity of the reaction product.

[S1] H. Gao, H.Yang, S. Wang, Hydrothermal synthesis, growth mechanism, optical properties and photocatalytic activity of cubic $SrTiO_3$ particles for the degradation of cationic and anionic dyes, *Optik*, 2018, **175**, 237-249.

[S2] F. Wang, H. Yang, Y. Zhang, Enhanced photocatalytic performance of $CuBi_2O_4$ particles decorated with Ag nanowires, *Mater. Sci. Semicond. Process.*, 2018, **73**, 58–66.

[S3] N. Daneshvar, D. Salari, A.. Khataee, Photocatalytic degradation of azo dye acid red 14 in water on ZnO as an alternative catalyst to TiO_2, *J. Photochem. Photobiol. Chem.*, 2004, **162**, 317–322.

[S4] S. Kansal, M. Singh, D. Sud, Studies on photodegradation of two commercial dyes in aqueous phase using different photocatalysts, *J. Hazard. Mater.*, 2007, **141**, 581–590.

[S5] Y. Wang, L. Rao, P. Wang, Z. Shi, L. Zhang, Photocatalytic activity of N-TiO_2/O-doped N vacancy g-C_3N_4 and the intermediates toxicity evaluation under tetracycline hydrochloride and Cr (VI) coexistence environment, *Appl. Catal. B: Environ.,* 2020, **262**, 118308.

[S6] W. Liu, Y. Li, F. Liu, W. Jiang, D. Zhang, J. Liang, Visible-light-driven photocatalytic degradation of diclofenac by carbon quantum dots modified porous g-C_3N_4: mechanisms, degradation pathway and DFT calculation, *Water Res.*, 2019, **151**, 8-19.

[S7] X. Hu, Y. Yu, D. Chen, W. Xu, J. Fang, Z. Liu, R. Li, Y. Li, J. Qin, Z. Fang, Anatase/Rutile homojunction quantum dots anchored on g-C_3N_4 nanosheets for antibiotics degradation in seawater matrice via coupled adsorption-photocatalysis: Mechanism insight and toxicity evaluation, *Chem. Eng. J.*, 2022, **432**, 134375.